Applied Catalysis B: Environmental 198 (2016) 16–24

Contents lists available at ScienceDirect

Applied Catalysis B: Environmental

journal homepage: www.elsevier.com/locate/apcatb

Bottlenecks limiting efficiency of photocatalytic water reduction by mixed Cd-Zn sulfides/Pt-TiO_2 composites

Anton Litke, Thomas Weber, Jan P. Hofmann*, Emiel J.M. Hensen*

Inorganic Materials Chemistry Group, Department of Chemical Engineering and Chemistry, Eindhoven University of Technology, P.O. Box 513, 5600 MB Eindhoven, The Netherlands

ARTICLE INFO

Article history:
Received 15 February 2016
Received in revised form 13 May 2016
Accepted 18 May 2016
Available online 19 May 2016

Keywords:
Sulfide
Titania
Photocatalysis
Hydrogen evolution
Composites

ABSTRACT

Visible-light driven photocatalytic water reduction on composite materials consisting of platinized titania (Pt-TiO_2) and transition metal sulfides (CdS or $Cd_{0.5}Zn_{0.5}S$) was investigated in detail. Sulfides were prepared by hydrothermal synthesis and room-temperature precipitation. The parameters limiting performance of these composite systems were elucidated. All composites with Pt-TiO_2 demonstrated similar hydrogen evolution rates independent from their textural properties, bandgaps, electron transfer between components and intrinsic activities of the sulfides. Moreover, all platinized sulfides, except for the precipitated CdS, were more active than the corresponding composites with Pt-TiO_2. This behavior – counterintuitive to the improved charge carrier separation found in the materials with heterojunctions – was rationalized by the low mobility of the conduction band electrons in TiO_2. The slow electron transport severely limits efficiency of the investigated composite materials in the photocatalytic water reduction. This effect is especially apparent for highly active sulfides but less so for materials with inherently low activity. The low driving force of bare CdS toward water reduction results in an apparent synergy with Pt-TiO_2 and makes the corresponding composites sensitive to Pt poisoning as the hydrogen evolution reaction predominantly takes place on Pt-TiO_2. On the other hand, mixed sulfides, being more active water reduction photocatalysts, compete with Pt particles in this process making corresponding composites less sensitive to the state of Pt. The findings are discussed in terms of the intrinsic photocatalytic activity of sulfides, electron transfer from sulfides to titania, electrochemical potentials of conduction band electrons, poisoning of Pt nanoparticles, and charge carrier mobility.

1. Introduction

The increasing global energy demand and environmental concerns related to utilization of fossil fuels are shifting attention toward other more sustainable energy sources. It is projected that in the near future a substantial fraction of the energy supply will be derived directly from the Sun [1]. However, the intermittent nature of solar energy necessitates the development of technologies for its storage and transport in a convenient form, *e.g.*, as liquid or gaseous chemical fuels such as H_2, hydrocarbons or alcohols. With respect to such chemical fuels, photocatalytic water splitting and reduction of carbon dioxide present a promising approach. These processes can in principle be carried out in one pot [2] and they can also be coupled with the oxidation of organic and inorganic waste [3,4]. However, most photocatalytic systems suffer from low energy conversion efficiency and stability issues and thus require substantial optimization.

The activity of photocatalytic systems depends on how efficiently photogenerated charge carriers are separated and utilized in the desired redox reactions. Different approaches have been developed to optimize the performance of photocatalytic systems. Among them are post-synthesis thermal treatment [5], surface modification [6], alloying or doping with different elements [5,7–9], loading of co-catalysts [10,11] and introduction of hetero- or homojunctions [12–15]. The combination of the latter two, which will be the topic of this paper, offers vast opportunities for system optimization, as co-catalysts increase the rate of surface redox reactions with the built-in electric field at the junctions enhancing electron-hole separation [16,18,19].

Among promising visible-light responsive composite photocatalytic systems such as $BiVO_4/WO_3$, $BiVO_4/ZnO$, Fe_2O_3/WO_3, $C_3N_4/SrTiO_3$ and others [16], we herein focus on composites of transition metal chalcogenides, *viz.* Cd-Zn sulfides, and TiO_2.

* Corresponding authors.
E-mail addresses: J.P.Hofmann@tue.nl (J.P. Hofmann), E.J.M.Hensen@tue.nl (E.J.M. Hensen).

http://dx.doi.org/10.1016/j.apcatb.2016.05.035
0926-3373/

Such composite systems have already been investigated for photocatalytic and photovoltaic applications over the last decades [12,13,16–18]. Our interest in sulfides arises from their tunable narrow bandgaps, which allow to utilize the visible (*e.g.*, CdS) and even near-IR (*e.g.*, PbS) parts of the solar spectrum. Transition metal sulfide-based systems can utilize H_2S, polysulfides or SO_2 as sacrificial reagents for photocatalytic hydrogen production, which can offer an environmentally benign solution for industrial waste treatment [3,4].

For CdS-TiO_2 composites it has been shown that photogenerated electrons are transferred from sulfide particles to the lower lying conduction band of titania [19]. This charge carrier separation increases the photocatalytic activity in comparison to the individual components [12,20,21]. Up to now, CdS-based composite photocatalysts have gained much more attention [13,18,21–23] than systems containing mixed Cd-Zn sulfides [20,24]. Mixed Cd-Zn sulfides, on the other hand, have higher activity toward photocatalytic water reduction than pure CdS. Although well studied, the origin of the higher activity of these mixed sulfides is not unequivocally established. In part, the upshift of the conduction band edge upon incorporation of Zn into the crystal lattice of CdS contributes to better performance. Overall, mixed Cd-Zn sulfides offer high flexibility for the development of photocatalytic materials because the positions of the valence and conduction bands with respect to H_2 and O_2 evolution levels, the bandgap (typically between 2.4 eV and 3.7 eV), and accordingly, the overall photocatalytic performance of the system can be adjusted by varying the Cd/Zn ratio [25–27].

Park and co-workers reported that the location of Pt co-catalyst particles in CdS-TiO_2 composites strongly influences the photocatalytic performance of the material. When Pt was solely present on TiO_2, the system was 3–30 times more active in photocatalytic water reduction than platinized CdS or when platinum was present on both components of the CdS-TiO_2 composite [28]. This approach has only been investigated for composites with CdS prepared by precipitation at room temperature [28,29]. We started our study from the premise that using more active mixed Cd-Zn sulfides instead of CdS should yield more active photocatalytic systems. The activity of a composite photocatalyst will depend on parameters such as light harvesting properties (bandgaps) and the intrinsic charge carrier separation efficiency of the semiconductors, the efficiency of charge carrier transfer between the two components, the electrochemical potentials of electrons and holes, the presence of co-catalysts, and the kinetics of the surface redox reactions [14]. Scheme 1 highlights these parameters for the envisioned $Cd_xZn_{1-x}S$@Pt-TiO_2 ($0 \le x \le 1$) photocatalyst system.

Herein, we investigated to what extent the efficiency of the visible-light driven photocatalytic water reduction on CdS- and $Cd_{0.5}Zn_{0.5}S$-based materials can be improved in a heterojunction with platinized TiO_2 (Aeroxide P25) and which parameters limit the overall efficiency of the resulting composite systems. For this purpose, CdS and $Cd_{0.5}Zn_{0.5}S$ were loaded on Pt-TiO_2 using either precipitation or a two-step hydrothermal synthesis approach. The photocatalytic activities of all composites with Pt-TiO_2 were very similar, counterintuitive to the notion of superior photocatalytic activity of the hydrothermally prepared sulfides, the efficient sulfide-to-titania electron transfer and the difference in optical and textural properties of materials. The photocatalytic activities of the composites with Pt-TiO_2 were significantly lower than those of the corresponding platinized sulfides for all materials, except for precipitated CdS. That is to say, the synergy earlier noted by Park and co-workers is not a generic feature of Cd-based sulfides in composite with titania. Detailed characterization and comparison of different model systems points out that the locus of the hydrogen evolution is different in the various composites. These salient differences also manifest themselves in higher sensitivity of the CdS-based systems to poisoning of the Pt co-catalyst.

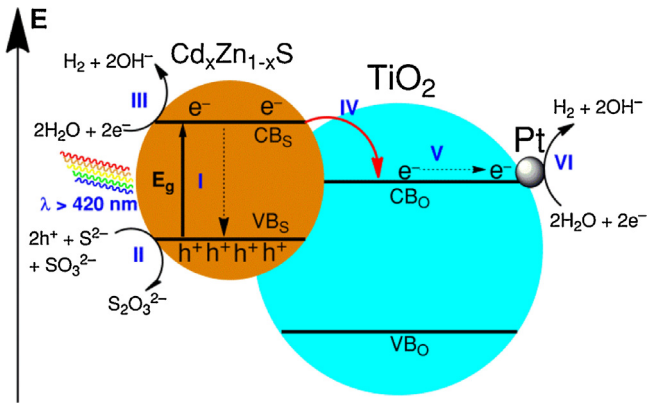

Scheme 1. Visible light-driven photocatalytic water reduction on $Cd_xZn_{1-x}S$@Pt-TiO_2 ($0 \le x \le 1$) composites in a mixed sulfide/sulfite sacrificial solution. Elementary steps include charge carrier generation and recombination in metal sulfide particles (I), oxidation of the sacrificial reagent (II) and water reduction (III) on sulfide particles, transfer of photo-generated electrons from the sulfide to TiO_2 (IV), diffusion of electrons in the TiO_2 particle to Pt (V) and water reduction on Pt (VI). Notations: e^- and h^+ – electrons and holes, E_g – bandgap; CB_s, CB_o, VB_s and VB_o – conduction bands and valence bands of sulfide and oxide, respectively.

2. Experimental

2.1. List of chemicals

$Cd(NO_3)_2{\cdot}4H_2O$ (Sigma Aldrich, ≥99%), $Zn(NO_3)_2{\cdot}6H_2O$ (Sigma Aldrich, ≥98%), NaOH (Sigma Aldrich, ≥98%), $Cd(CH_3COO)_2{\cdot}2H_2O$ (Sigma Aldrich, ≥98%), $Zn(CH_3COO)_2{\cdot}2H_2O$ (Sigma Aldrich, ≥98%), thioacetamide (Sigma Aldrich, >99%), CH_3COONa (Sigma Aldrich, ≥99%), $Na_2S{\cdot}9H_2O$ (Sigma Aldrich, ≥98%), Na_2SO_3 (Sigma Aldrich, 98–100%), $H_2PtCl_6{\cdot}nH_2O$ (Sigma-Aldrich, ≥38% Pt basis), CO gas (The Linde Group, ≥99.995%) and absolute ethanol (VWR, technical grade) were used as received without further purification. Demineralized water (>15 MΩ cm at 25 °C) was used for the preparation of solutions, as a solvent for synthesis and to wash the samples.

2.2. Sample preparation

CdS and $Cd_{0.5}Zn_{0.5}S$ sulfides were prepared by either hydrothermal synthesis from insoluble hydroxides and thioacetamide in 1.0 M CH_3COONa or by precipitation from an aqueous Na_2S solution at room temperature. Commercial TiO_2 (Evonik, Aeroxide P25) was used in all experiments.

2.2.1. Hydrothermal synthesis of Cd and Cd-Zn sulfides

CdS and $Cd_{0.5}Zn_{0.5}S$ were prepared according to a modified procedure described in literature [30]. First, insoluble hydroxides were precipitated by adding aqueous NaOH (15 mL, 8.2×10^{-3} mol) to aqueous solutions of either $Cd(NO_3)_2 \times 4H_2O$ (30 mL, 4.1×10^{-3} mol) or $Cd(NO_3)_2 \times 4H_2O$ and $Zn(NO_3)_2 \times 6H_2O$ (30 mL, 2.05×10^{-3} mol each salt). The white suspension was stirred for 15 min and the precipitate was separated by centrifugation, washed three times with demineralized water and re-dispersed in 35 mL 1.0 M CH_3COONa in a PTFE-lined stainless steel autoclave (45 mL capacity). Then 4.51×10^{-3} mol thioacetamide (10% sulfur excess) was added to this dispersion under stirring, the autoclave was sealed, placed in an oven and heated to 180 °C under continuous tumbling. After 24 h the autoclave was rapidly cooled to room temperature and the solid product was collected by centrifugation, washed three times with demineralized water, once with ethanol and dried under vacuum at room temperature. The dried material was ground, weighed and stored in

a glass vial. The samples prepared via this method are denoted as h-CdS and h-$Cd_{0.5}Zn_{0.5}S$.

2.2.2. Precipitation of Cd and Cd-Zn sulfides

CdS and $Cd_{0.5}Zn_{0.5}S$ were prepared by simple precipitation at room temperature according to the following procedure. For CdS, 4.1×10^{-3} mol $Cd(CH_3COO)_2{\cdot}2H_2O$ was dissolved in 30 mL demineralized water, then 41 mL 0.1 M Na_2S was added dropwise to this solution under vigorous stirring. The suspension was stirred for 30 min. The solid was collected by centrifugation, washed three times with demineralized water, once with ethanol and dried under vacuum at room temperature. Preparation of $Cd_{0.5}Zn_{0.5}S$ was done similarly from a solution containing $Cd(CH_3COO)_2{\cdot}2H_2O$ and $Zn(CH_3COO)_2{\cdot}2H_2O$ (2.05×10^{-3} mol each salt). These samples are denoted as p-CdS and p-$Cd_{0.5}Zn_{0.5}S$.

2.2.3. Pt photodeposition on metal sulfides

p-CdS, p-$Cd_{0.5}Zn_{0.5}S$, h-CdS and h-$Cd_{0.5}Zn_{0.5}S$ were loaded with 0.5 wt.% Pt (nominal loading) using a method described in literature [10]. Briefly, 100 mg of the sulfide sample was dispersed under sonication in 50 mL 1.0 M NaOH containing 0.5 mg Pt (in the form of H_2PtCl_6). The dispersion was transferred into a side-illuminated PEEK photocatalytic cell, degassed and irradiated for 3 h under continuous stirring. A 500 W Hg(Xe) lamp (Newport) equipped with an IR-filter (demineralized water) and a 420 nm cut-off filter ($OD^{410} = 5.0$, Newport) was used as the light source. After irradiation, the solid was separated by centrifugation, washed three times with demineralized water and dried at room temperature under vacuum.

2.2.4. Hydrothermal synthesis of Cd and Cd-Zn sulfide-titania composites

Composites were prepared according to the following procedure. First, 4.1×10^{-3} mol $Cd(NO_3)_2{\cdot}4H_2O$ or a mixture of 2.05×10^{-3} mol $Cd(NO_3)_2{\cdot}4H_2O$ and 2.05×10^{-3} mol $Zn(NO_3)_2{\cdot}6H_2O$ was dissolved in 30 mL demineralized water. Then TiO_2 or Pt-TiO_2 (0.59 g for CdS or 0.5 g for $Cd_{0.5}Zn_{0.5}S$) was dispersed in this solution under sonication and 25 mL aqueous NaOH (8.2×10^{-3} mol) was added dropwise under continuous stirring. The mixture was stirred for 15 min and then separated by centrifugation, washed twice with demineralized water and redispersed in 35 mL 1.0 M CH_3COONa in a PTFE-lined stainless steel autoclave (45 mL capacity). Finally, 4.51×10^{-3} mol thioacetamide (10% sulfur excess) was added to this dispersion under stirring. The autoclave was then sealed and subjected to hydrothermal treatment. Product collection was identical to the procedure used in hydrothermal synthesis of sulfides. The resulting samples are denoted as h-CdS@TiO_2, h-CdS@Pt-TiO_2, h-$Cd_{0.5}Zn_{0.5}S$@TiO_2 and h-$Cd_{0.5}Zn_{0.5}S$@Pt-TiO_2.

2.2.5. Precipitation of Cd and Cd-Zn sulfide-titania composites

First, 4.1×10^{-3} mol $Cd(NO_3)_2{\cdot}4H_2O$ or a mixture of 2.05×10^{-3} mol $Cd(NO_3)_2{\cdot}4H_2O$ and 2.05×10^{-3} mol $Zn(NO_3)_2{\cdot}6H_2O$ was dissolved in 30 mL demineralized water. Then TiO_2, Pt-TiO_2 or s-Pt-TiO_2 (0.59 g for CdS or 0.5 g for $Cd_{0.5}Zn_{0.5}S$) was dispersed in this solution under sonication and 41 mL of an aqueous 0.1 M Na_2S solution was added dropwise under vigorous stirring to the suspensions. The obtained slurry was stirred for 15 min and separated by centrifugation, washed three times with demineralized water, once with ethanol and dried at room temperature under vacuum. The samples obtained with this method are denoted as p-CdS@TiO_2, p-$Cd_{0.5}Zn_{0.5}S$@TiO_2, p-CdS@s-Pt-TiO_2, p-$Cd_{0.5}Zn_{0.5}S$@s-Pt-TiO_2, p-CdS@Pt-TiO_2 and p-$Cd_{0.5}Zn_{0.5}S$@Pt-TiO_2.

2.2.6. Photodeposition of Pt on TiO_2

TiO_2 was loaded with 0.5 wt.% Pt according to the following procedure. 0.5 g of titania was dispersed in 90 mL of an aqueous solution containing 10 vol.% CH_3OH and 2.5 mg Pt (in the form of H_2PtCl_6). The dispersion was transferred and degassed in a double-walled glass photocatalytic reactor with top-mounted quartz window. During photodeposition the mixture was kept at 20 °C using a thermostated bath. A 500 W Hg(Xe) lamp (Newport) equipped with an IR-filter (demineralized water) and a full spectrum turning mirror (200 nm – 30 μm spectral range) was used as the light source. After 1 h irradiation a grey product was separated from the mother solution by centrifugation, washed three times with demineralized water and dried under vacuum at room temperature.

2.2.7. Poisoning of Pt-TiO_2

Model poisoning was carried out by subjecting Pt-TiO_2 to hydrothermal treatment in the presence of H_2S. First, 0.5 g Pt-TiO_2 (0.5 wt.% nominal Pt content) was dispersed in 35 mL 1.0 M CH_3COONa in a PTFE-lined autoclave. Then 4.5×10^{-4} mol thioacetamide (represents 10% sulfur excess used in hydrothermal synthesis of sulfides and composites) was added to the dispersion and the autoclave was sealed and kept at 180 °C in the oven under tumbling. After 24 h the autoclave was cooled to room temperature. The resulting solid was collected by centrifugation, washed three times with demineralized water and dried under vacuum at room temperature. The sample is denoted as s-Pt-TiO_2.

2.3. Characterization

Samples were characterized by means of TEM, XRD, XPS, N_2 physisorption, ICP-OES, room-temperature steady-state photoluminescence, UV–vis and FTIR spectroscopy. Bright field TEM images were acquired on a FEI Technai G2 (type Sphera, LaB_6, 200 kV) transmission electron microscope. X-ray diffractograms were recorded on a Bragg-Brentano Bruker Endeavour D2 powder diffractometer equipped with a Cu cathode and a 1D LYNXEYE detector, Ni filter, 1.0 mm primary beam slit and 3.0 mm height beam knife. The diffractograms were recorded in the 10–60° 2θ range with steps of 0.032°. X-ray photoelectron spectra were obtained on a Thermo K-Alpha spectrometer equipped with a monochromated Al Kα X-ray source. Spectra of individual elements were recorded at 0.1 eV resolution, a dwell time of 50 ms and by averaging 10–30 individual scans depending on the element content and signal intensity. Steady-state photoluminescence spectra of sulfides, TiO_2 and composite photocatalysts were recorded at room temperature with an ANDOR Shamrock 500 UV–vis spectrograph equipped with an ANDOR Newton EMCCD camera. The samples were irradiated by the 325 nm line of a He-Cd laser. Bandgaps of the materials were determined on the basis of diffuse-reflectance UV–vis spectra recorded on a UV–vis spectrometer (Shimadzu UV-2401PC) equipped with an integrating sphere accessory. $BaSO_4$ was used as the reference material. The BET surface areas of the samples were determined from N_2 physisorption isotherms measured on an ASAP Tristar II module. Room-temperature CO adsorption was carried out in a three-window in-situ low-temperature diffuse reflectance optical cell (Praying Mantis, Harrick Scientific). IR spectra were recorded on a Bruker Vertex 70v FTIR spectrometer in reflectance mode at 4 cm^{-1} resolution by averaging 100 scans using a liquid nitrogen-cooled MCT detector. KBr (Sigma Aldrich, FT-IR grade) was used as the reference material. Detailed description of the experimental procedures and data analysis can be found in the Supplementary Information.

Table 1
Properties of Cd and Cd-Zn sulfides and their composites with (Pt-)TiO_2.

Sample	Photocatalytic activity[a], μmol(H_2)/h	S_{BET}, m^2/g	Bandgap[b], eV
h-$Cd_{0.5}Zn_{0.5}S$	130	26	2.59
h-$Cd_{0.5}Zn_{0.5}S$@TiO_2	105	38	2.55
h-$Cd_{0.5}Zn_{0.5}S$@Pt-TiO_2	70	39	2.58
h-CdS	8	12	2.41
h-CdS@TiO_2	6	32	2.38
h-CdS@Pt-TiO_2	20	37	2.35
p-$Cd_{0.5}Zn_{0.5}S$	40	145	2.67
p-$Cd_{0.5}Zn_{0.5}S$@TiO_2	40	123	2.67
p-$Cd_{0.5}Zn_{0.5}S$@Pt-TiO_2	50	124	2.62
p-CdS	15	140	2.38
p-CdS@TiO_2	28	102	2.47
p-CdS@Pt-TiO_2	52	89	2.43
TiO_2	N.A.	53	3.21
Pt-TiO_2	N.A.	52	3.04
s-Pt-TiO_2	N.A.	49	2.98

[a] hydrogen evolution rates under visible light irradiation (λ > 420 nm); 10 mg of sulfides or 20 mg of composites in 50 mL 0.25 M Na_2S + 0.35 M Na_2SO_3 sacrificial solution.
[b] bandgaps of composites correspond to direct allowed bandgaps of the sulfide phases; values reported for (Pt-)TiO_2 correspond to indirect allowed transitions.

2.4. Photocatalytic activity measurements

Photocatalytic activity measurements were carried out in a gas-tight photocatalytic setup connected to an online GC-TCD (ShinCarbon column, N_2 carrier gas). In each test 10 mg of sulfides was used (*i.e.*, 10 mg of bare sulfides or 20 mg of composites). The sample was dispersed by sonication in the 50 mL sacrificial solution (0.25 M Na_2S + 0.35 M Na_2SO_3). This dispersion was transferred to a side-illuminated PEEK cell and degassed. The 500 W Hg(Xe) lamp (Newport) equipped with an IR-filter (demineralized water) and a 420 nm cut-off filter (OD^{410} = 5.0, Newport) was used for the photocatalytic activity measurements. A light intensity controller (model 68950, Newport) was used to maintain constant light flux in all experiments. The temperature in the double-walled cell was maintained at 20 °C using a thermostated bath. Gaseous products were automatically sampled by the gas chromatograph with 12 min intervals. The values reported in this study are averages of several sequential photocatalytic runs (1.5–2.0 h each).

3. Results and discussion

The photocatalytic activity of the composite prepared by hydrothermal deposition of mixed Cd-Zn sulfide on Pt-TiO_2 (0.5 wt.% Pt on TiO_2) was found to be half of that of the standalone sulfide prepared by the same method (Table 1). This result is different from the substantial increase of the photocatalytic activity reported for the CdS-containing system prepared by room-temperature precipitation [28,29]. The lower performance of h-$Cd_{0.5}Zn_{0.5}S$@Pt-TiO_2 cannot be attributed to light scattering or shading by grey Pt-TiO_2 as the activities of h-$Cd_{0.5}Zn_{0.5}S$ and its physical mixture with Pt-TiO_2 were the same (Fig. S1, Supplementary Information). In order to understand the reason for this substantial difference, we systematically studied how the activity of composite photocatalysts correlates with the properties of the sulfide component. To this end, standalone CdS, $Cd_{0.5}Zn_{0.5}S$ and their composites with (Pt-)TiO_2 were prepared using two different methods, namely hydrothermal synthesis [30] and room-temperature precipitation [28], denoted by prefixes *h-* and *p-*, respectively. Results of photocatalytic activity tests, bandgaps and BET surface areas of these samples are summarized in Table 1. Fig. 1 represents powder XRD patterns of these materials.

One can see that the material properties depended significantly on the preparation method. The precipitated samples showed much

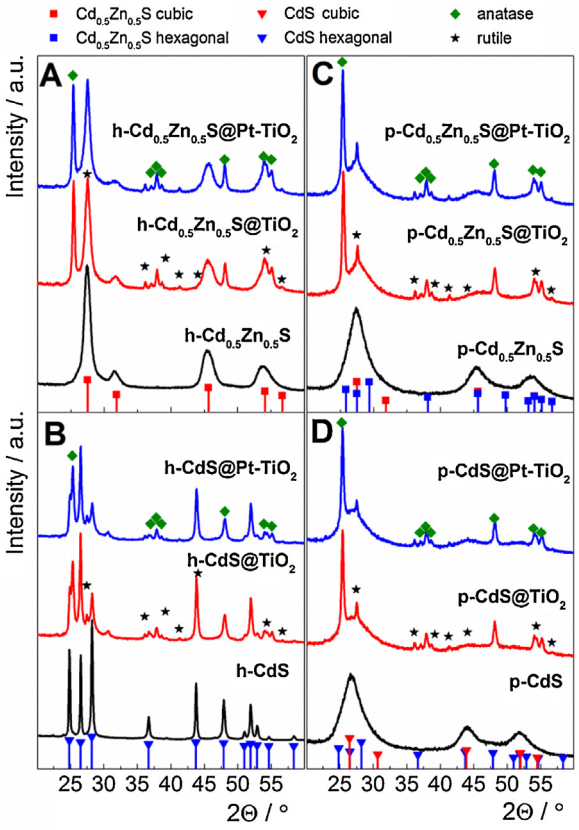

Fig. 1. X-ray diffractograms of bare sulfides and composite photocatalysts based on h-$Cd_{0.5}Zn_{0.5}S$ (A), h-CdS (B), p-$Cd_{0.5}Zn_{0.5}S$ (C), and p-CdS (D) and the reference XRD patterns.

broader XRD reflections and higher BET surface areas than the hydrothermally prepared samples. As expected, h-$Cd_{0.5}Zn_{0.5}S$ and p-$Cd_{0.5}Zn_{0.5}S$ had larger bandgaps (Table 1) and their XRD reflections were shifted toward higher 2θ values as compared with CdS (Fig. 1). These differences evidence the incorporation of Zn into the CdS lattice and formation of solid solutions [31]. The XRD patterns of h-CdS and h-$Cd_{0.5}Zn_{0.5}S$ (Fig. 1A and B) agreed well with the results of our previous work [30]. In brief, h-CdS is composed of the hexagonal crystal phase and has a well-defined XRD pattern. This CdS phase is known to have higher photocatalytic activity than the other polymorph [32,33]. h-$Cd_{0.5}Zn_{0.5}S$ is obtained with cubic crystal structure and its XRD pattern contains broader reflections due to the compositional inhomogeneities in mixed Cd-Zn sulfides [30]. Very broad diffraction lines hampered accurate assignment of the crystal phases present in p-CdS and p-$Cd_{0.5}Zn_{0.5}S$. The main reason for this line broadening is the small size of coherently scattering domains in precipitated sulfides. Application of the Scherrer equation [34] allowed estimating the crystallite sizes to be 2.2 and 2.5 nm for p-CdS and p-$Cd_{0.5}Zn_{0.5}S$, respectively. These values are in good agreement with TEM data (Fig. S2, Supplementary Information) and the consistently larger BET surface areas of the precipitated samples (Table 1). In principle, other phenomena like distortion of the unit cell due to the presence of crystal defects or compositional inhomogeneities can also contribute to this line broadening [30,35–37], but this cannot be properly assessed on the basis of the present data. The composites with (Pt-)TiO_2 exhibited complex XRD patterns of mixed-phase TiO_2 P25 and sulfide components (Fig. 1). The crystal phase composition of sulfides in composite materials was the same as in standalone materials. The only apparent difference was the intensity change observed for the

Table 2
Comparison of the intrinsic photocatalytic activities of transition metal sulfides.

Sample	Normalized photocatalytic activity[a], μmol(H_2)/(h × m^2)	Photocatalytic activity[b], μmol(H_2)/h
h-$Cd_{0.5}Zn_{0.5}S$	500	125
h-CdS	66.7	113
p-$Cd_{0.5}Zn_{0.5}S$	27.6	80
p-CdS	10.7	40

[a] Activities of bare sulfides normalized to BET surface areas.
[b] Activities of sulfides loaded with 0.5 wt.% Pt (nominal amount).

main XRD reflections of hexagonal h-CdS in the composite materials compared to the bare sulfide (Fig. 1B).

3.1. Relationship between activities of sulfides and composite photocatalysts

Among the bare sulfides, the hydrogen evolution rates increase in the order h-CdS < p-CdS < p-$Cd_{0.5}Zn_{0.5}S$ < h-$Cd_{0.5}Zn_{0.5}S$ (Table 1). It is usually found that photocatalytic activity is higher for samples of increasing crystallinity [13]. This holds true for mixed metal sulfides but not for CdS samples. However, when hydrogen evolution rates of the bare sulfides were normalized to their BET surface areas the superior photocatalytic activity of hydrothermal samples became apparent revealing the anticipated trend of p-CdS < p-$Cd_{0.5}Zn_{0.5}S$ < h-CdS ≪ h-$Cd_{0.5}Zn_{0.5}S$ (Table 2).

Another approach to appraise the difference between bare sulfides prepared by different methods is to improve charge carrier separation and increase the rate of hydrogen production using an efficient co-catalyst such as Pt, which has low overpotential for the hydrogen evolution reaction [10,38]. Loading of Pt on bare sulfides can compensate for the difference in electrochemical potential of the conduction band electrons in CdS and $Cd_{0.5}Zn_{0.5}S$, which then allows for direct comparison of their intrinsic efficiencies based on the hydrogen evolution rates. It has been demonstrated that the photocatalytic activity of platinized CdS strongly depends on the Pt deposition method [10]. Therefore, we adopted an optimized procedure reported in literature in order to load 0.5 wt.% Pt on precipitated and hydrothermal sulfides. Photocatalytic activities of these samples are summarized in Table 2. The activity trend of platinized sulfides agrees with the normalized hydrogen evolution rates and confirms the superior activity of the hydrothermally prepared sulfides. Nonetheless, these trends do not correlate with the fact that h-CdS@Pt-TiO_2 was the least active composite in the series with 2.5-times lower performance than p-CdS@Pt-TiO_2. Moreover, the performance of p-CdS@Pt-TiO_2 and p-$Cd_{0.5}Zn_{0.5}S$@Pt-TiO_2 were identical despite the difference in their bandgaps (Table 1) and the intrinsic activities of sulfides (Table 2). Thus, we surmise that neither the intrinsic efficiency of sulfides nor their optical properties determine photocatalytic activity of the composites with Pt-TiO_2.

3.2. Electron transfer from sulfides to TiO_2

Besides light harvesting properties and activities of sulfides, the performance of the composite photocatalysts depends on electron transfer from the conduction band of sulfide to titania (process IV, Scheme 1). This parameter can be assessed by comparing activities of sulfides and composites with bare and platinized TiO_2. From Table 1 one observes that both h-CdS@TiO_2 and h-$Cd_{0.5}Zn_{0.5}S$@TiO_2 were less active than the corresponding bare sulfides. This activity decrease indicates that there is a good contact between sulfide and TiO_2 particles in these composites and an appreciable part of the electrons generated by above-bandgap excitation of the sulfide is transferred to TiO_2 [19]. As bare titania has low activity toward the water reduction reaction, this electron transfer lowers the photocatalytic activity of the composite. The improved charge carrier separation in hydrothermal composites was further confirmed by quenched photoluminescence of sulfides [11] in the composite samples (Fig. S4, Supporting Information). The observed efficient electron transfer agrees with h-CdS@Pt-TiO_2 being 2.5-times more active than h-CdS, but it fails to explain the deteriorated activity of h-$Cd_{0.5}Zn_{0.5}S$@Pt-TiO_2 (Table 1).

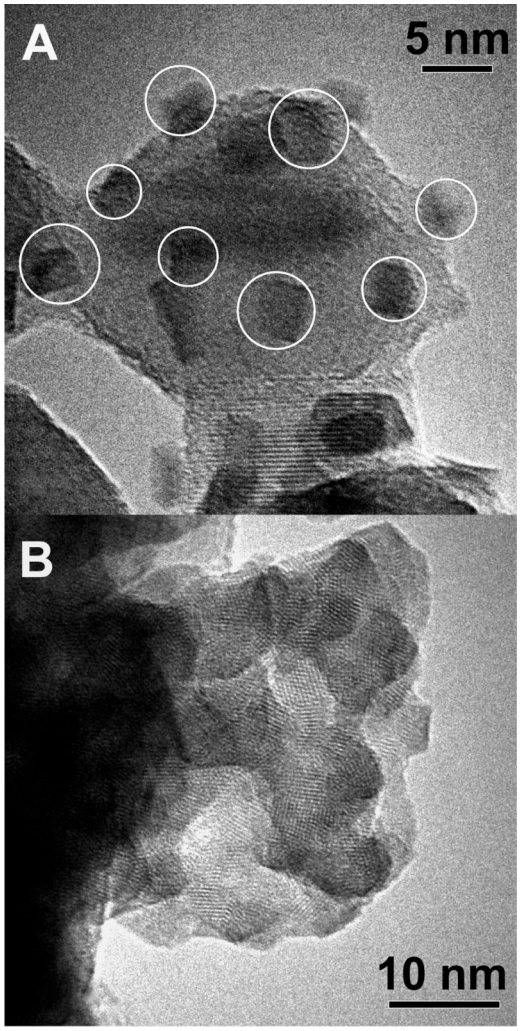

Fig. 2. TEM images of p-CdS@TiO_2. (A) p-CdS particles (white circles) anchored on TiO_2; (B) an aggregate of p-CdS crystallites.

Precipitated samples showed different behavior. p-CdS@TiO_2 was almost twice as active as p-CdS, whereas activities of p-$Cd_{0.5}Zn_{0.5}S$ and p-$Cd_{0.5}Zn_{0.5}S$@TiO_2 were the same. The higher activity of p-CdS@TiO_2 can be rationalized as follows. First of all, hydrogen evolution rates of p-CdS and its physical mixture with TiO_2 were identical (Fig. S1, Supplementary Information), which excludes light scattering on TiO_2 as the reason for the enhanced activity of p-CdS@TiO_2. Secondly, as discussed above, efficient transfer of electrons from sulfides to bare TiO_2 should not be expected to increase photocatalytic activity of this composite. On the other hand, the apparent activity of bare CdS strongly depends on the exposed surface area, which is most evident for bare h-CdS and p-CdS (Table 1). From the TEM images of p-CdS@TiO_2 one can see that sulfide crystallites were deposited on TiO_2 particles, which prevented their aggregation (Fig. 2). Therefore, higher activity of this sample is attributed to the improved dispersion of the sulfide.

In contrast to p-CdS, loading of sulfide on titania does not have a positive effect on p-$Cd_{0.5}Zn_{0.5}S$ (Table 1). This distinct behavior

of mixed Cd-Zn sulfides and pure CdS loaded on TiO_2 can be understood from the difference of the conduction band potentials and kinetics of the water reduction reaction on these materials. Bare CdS exhibits low driving force toward water reduction and its activity strongly depends on the exposed surface area. On the other hand, the mixed Cd-Zn sulfides have higher photocatalytic activity due to the higher energy of the conduction band [25,26]. Faster kinetics of water reduction reaction on $Cd_{0.5}Zn_{0.5}S$ make them less sensitive to the dispersion of sulfide particles on titania, resulting in similar activities of p-$Cd_{0.5}Zn_{0.5}S$ and p-$Cd_{0.5}Zn_{0.5}S$@TiO_2.

When p-CdS@Pt-TiO_2 and p-$Cd_{0.5}Zn_{0.5}S$@Pt-TiO_2 are included in this comparison, one can see that the activity increases in the order sulfide ≤ composite with TiO_2 < composite with Pt-TiO_2 (Table 1). The difference in activity is much higher for the p-CdS-based system (three-fold increase) than for the mixed sulfide (25% improvement). Similar to the previous case, this discrepancy can be explained by the low energy of the conduction band electrons in CdS [39]. The heterojunction with Pt-TiO_2 opens a pathway for efficient utilization of photogenerated electrons by transferring them from p-CdS to TiO_2 and further to Pt sites where they can facilitate the hydrogen evolution reaction with low overpotentials [28,38]. This leads to a three-fold increase of photocatalytic activity (Table 1) consistent with the findings of Park et al. [28]. Mixed sulfide particles, having a more negatively positioned conduction band [25,26], compete with Pt centers in the water reduction reaction. Thus, most of the hydrogen is produced on the sulfide component of p-$Cd_{0.5}Zn_{0.5}S$@Pt-TiO_2 and not on Pt-TiO_2 which results in a less prominent activity increase. More evidence supporting this hypothesis is provided in Section 3.4.

3.3. Poisoning of Pt co-catalyst

The electron transfer from sulfides to TiO_2 was indirectly found to be more efficient in hydrothermally prepared composites than in the precipitated counterparts. However, this cannot explain why the activity of h-$Cd_{0.5}Zn_{0.5}S$@Pt-TiO_2 was just half of the h-$Cd_{0.5}Zn_{0.5}S$ activity and why h-CdS@Pt-TiO_2 was the least active composite containing Pt-TiO_2 (Table 1). Taking into account the observed discrepancies one can suggest that the Pt co-catalyst was affected by the hydrothermal treatment.

The core level binding energies of Zn, Cd, S, Ti and O were similar for all composites irrespective of the preparation method (Table S1, Supplementary Information). Reliable analysis of the Pt state in the composites was complicated by the low metal content (ca. 0.25 wt.% Pt, Table S2, Supplementary Information) and the overlap of Pt 4f and Cd 4p core level lines [40]. To evaluate the influence of the hydrothermal treatment on the Pt co-catalyst, we analyzed and compared two Pt-TiO_2 samples. One sample was used as prepared (Pt-TiO_2), while the other (s-Pt-TiO_2) was subjected to a hydrothermal treatment resembling the synthesis of composites: 24 h, 180 °C, 1.0 M CH_3COONa in the presence of 4.1×10^{-4} mol thioacetamide. This amount of thioacetamide represents 10% excess of sulfur used in synthesis, which is expected to be in contact with Pt particles over a long period of time while the rest forms insoluble sulfides. The Pt 4f XPS spectra of Pt-TiO_2 and s-Pt-TiO_2 are shown in Fig. 3. The asymmetric line shapes and low binding energies evidence the presence of metallic Pt. The binding energy of Pt $4f_{7/2}$ line was slightly higher for the sample subjected to the hydrothermal treatment (70.3 and 70.6 eV for Pt-TiO_2 and s-Pt-TiO_2, respectively). Both values were lower than the binding energy of the Pt $4f_{7/2}$ line in polycrystalline metal samples (ca. 71.0 eV) [41], yet agreed well with the values reported for supported Pt nanoparticles [42,43]. The presence of small Pt nanoparticles in these samples was confirmed by TEM analysis, which returned 2.2 nm and 2.3 nm for the mean size of Pt particles in Pt-TiO_2 and s-Pt-TiO_2 samples, respectively (Fig. S5, Supplementary Information). This difference in particle

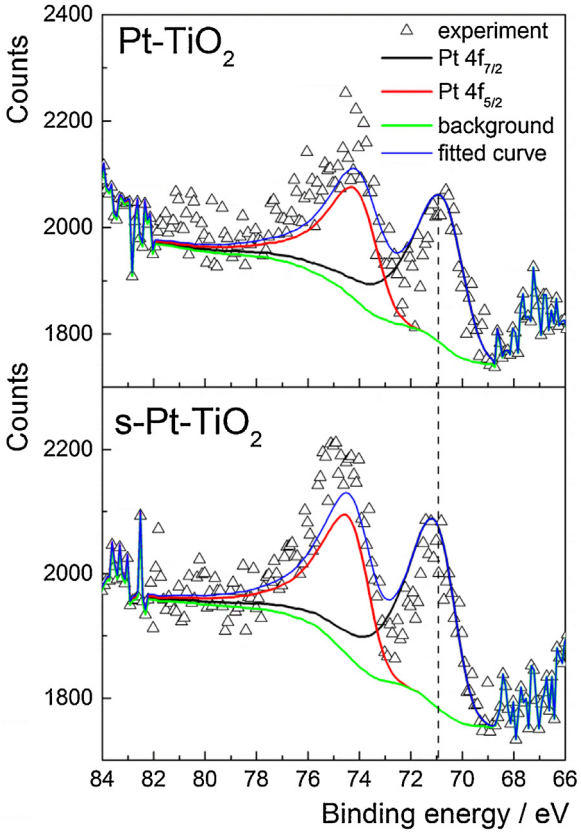

Fig. 3. Pt 4f core-level X-ray photoelectron spectra of 0.5 wt.% Pt-TiO_2 samples: as-prepared (top) and poisoned (bottom).

sizes could account for the observed differences in binding energies. The atomic Pt-to-Ti ratio, as extracted from the normalized areas of Ti $2p_{3/2}$ and Pt $4f_{7/2+5/2}$ lines, was similar in both samples, *i.e.* 0.0074 for Pt-TiO_2 and 0.0071 for s-Pt-TiO_2. This agreed well with the results of the ICP-OES elemental analysis (Table S2, Supplementary Information) and confirmed that the hydrothermal treatment did not cause leaching of platinum. Moreover, no sulfur was detected by XPS in either of the samples, setting its amount to below the detection limit of the instrument, which is expected to be around 1.0 wt.% for light elements.

Given the probing depth of XPS and the mean Pt particle size of 2.2–2.3 nm (Fig. S5, Supplementary Information), XPS data shown in Fig. 4 reflect the bulk of the Pt particles rather than only their surface. Thus, we explored CO adsorption in an FTIR analysis to selectively probe the surface of the co-catalysts before and after the hydrothermal treatment (Fig. 4). At room temperature carbon monoxide strongly adsorbs on metallic Pt [44,45] but not on TiO_2 [46]. The adsorption on Pt results in the appearance of a distinctive IR band in the 2100–2050 cm^{-1} spectral region [44,45].

When Pt-TiO_2 was exposed to 0.13 mbar CO, three bands emerged in the IR spectrum: main bands at 2063 cm^{-1} and 1830 cm^{-1} along with a small sharp band at 2115 cm^{-1} (Fig. 4A). The bands at 2063 cm^{-1} and 1830 cm^{-1} correspond to linear and bridged adsorption of CO on Pt^0 [44,45]. The band at 2115 cm^{-1} can be assigned to CO adsorbed on isolated Pt atoms [47]. The behavior of s-Pt-TiO_2 in response to CO exposure was different. No bands were observed at 0.1 mbar CO and only a very weak band appeared at 2104 cm^{-1} when the partial pressure of CO was increased to 1.0 mbar (Fig. 4B). The band position and its low intensity indicate that the surface of Pt particles was no longer metallic after hydrothermal treatment. It might be that a PtS surface layer formed [48]. Similar to s-Pt-TiO_2, no bands of CO adsorbed on metallic Pt

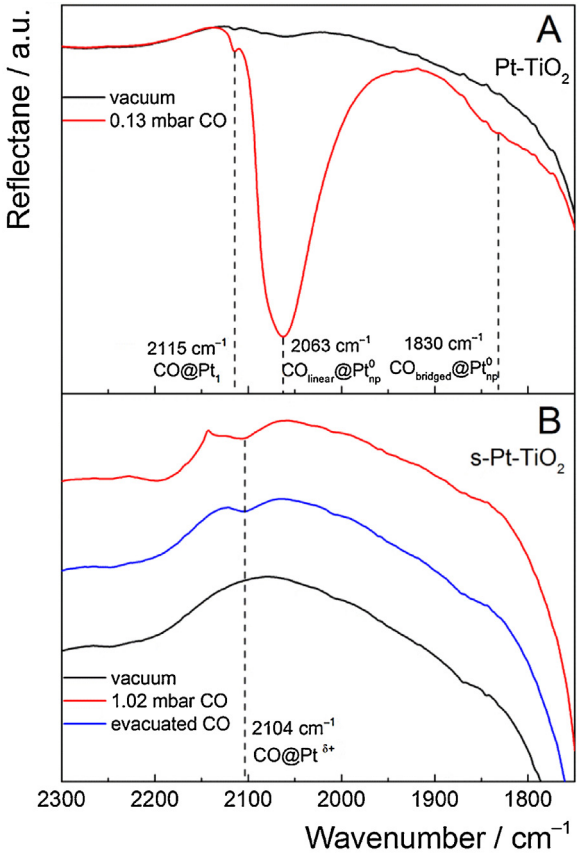

Fig. 4. DRIFT spectra of Pt-TiO_2 (A) and s-Pt-TiO_2 (B) in the presence of CO. Notations of the platinum species: Pt^0_{np} – metallic nanoparticles, Pt_1 – isolated atoms, $Pt^{\delta+}$ – oxidized species.

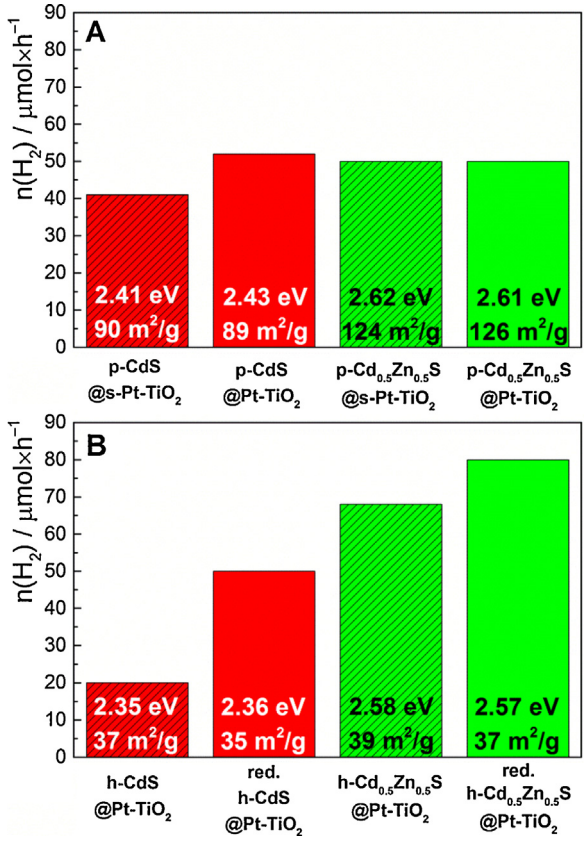

Fig. 5. Results of the photocatalytic activity tests, bandgaps and BET surface areas of the composites containing poisoned (patterned bars) or metallic (solid bars) Pt nanoparticles. (A) materials prepared by co-precipitation, (B) materials prepared by hydrothermal synthesis.

were detected for h-$Cd_{0.5}Zn_{0.5}S$@Pt-TiO_2 (Fig. S6, Supplementary Information). Hence, poisoning of hydrogen evolution sites (*i.e.*, Pt nanoparticles) can explain why h-CdS@Pt-TiO_2 was less active than p-CdS@Pt-TiO_2 and why the activity of h-$Cd_{0.5}Zn_{0.5}S$@Pt-TiO_2 was significantly lower than that of the corresponding bare sulfide (Table 1).

3.4. Effect of Pt poisoning on the activities of composite photocatalysts

In order to evaluate how Pt poisoning influenced the performance of different composite photocatalysts, we reduced h-CdS@Pt-TiO_2 and h-$Cd_{0.5}Zn_{0.5}S$@Pt-TiO_2 in a mixed flow of H_2 (5 mL/min) and He (25 mL/min) for 3 h at 300 °C. In addition, p-CdS@s-Pt-TiO_2 and p-$Cd_{0.5}Zn_{0.5}S$@s-Pt-TiO_2 (composite photocatalysts with poisoned s-Pt-TiO_2) were prepared by room temperature precipitation to further evaluate the electron transfer efficiency in these composites and to elucidate whether the hydrogen evolution reaction predominantly takes place on Pt-TiO_2 or on sulfide particles. Photocatalytic activities, BET surface areas and bandgaps of these samples are shown in Fig. 5. XRD patterns of the samples are represented in Fig. S7, Supplementary Information. Pt poisoning influenced the performance of composites with CdS and $Cd_{0.5}Zn_{0.5}S$ in different ways. p-CdS@s-Pt-TiO_2 was 25% less active than p-CdS@Pt-TiO_2, while the activities of p-$Cd_{0.5}Zn_{0.5}S$@s-Pt-TiO_2 and p-$Cd_{0.5}Zn_{0.5}S$@Pt-TiO_2 were identical (Fig. 5A). Hydrothermally prepared samples behaved similar. Reduction of Pt increased activity of h-CdS@Pt-TiO_2 from 20 to 50 µmol(H_2)/h, but had only a minor effect on h-$Cd_{0.5}Zn_{0.5}S$@Pt-TiO_2 (Fig. 5B) despite the fact that the presence of metallic Pt in this sample was confirmed by FTIR analysis (Fig. S6, Supplementary Information).

These results are in line with the earlier formulated conclusions. First of all, the presence of active hydrogen evolution sites is important for photocatalytic water reduction on CdS-based composites, which makes them more sensitive to S poisoning of Pt. The minor influence of Pt-poisoning on the activity of the composites containing $Cd_{0.5}Zn_{0.5}S$ supports the hypothesis that on these composite photocatalysts hydrogen production predominantly takes place on sulfide particles rather than on Pt-TiO_2. Secondly, Pt poisoning had a more prominent effect on the activities of hydrothermally prepared composites than on their precipitated counterparts (Fig. 5). This agrees with the fact that in hydrothermally prepared composites a large fraction of photogenerated electrons is transferred from the sulfide to titania. These electrons can only facilitate the water reduction reaction on Pt particles due to the low activity of bare TiO_2 towards the hydrogen evolution reaction. Therefore, the more efficient the electron transfer is, the more sensitive the system becomes to co-catalyst poisoning.

3.5. Parameters limiting photocatalytic activity of the composite materials

Fig. 5 shows that photocatalytic activities of p-CdS@Pt-TiO_2, p-$Cd_{0.5}Zn_{0.5}S$@Pt-TiO_2 and reduced h-CdS@Pt-TiO_2 were almost identical (ca. 50 µmol/h), and only h-$Cd_{0.5}Zn_{0.5}S$@Pt-TiO_2 showed better performance. The activity trends did not correlate with the light harvesting properties of the materials (Table 1), the intrinsic activities of the sulfide components (Table 2) nor the efficiency of electron transfer from sulfides to TiO_2. This rules out that these

parameters limit the overall performance of the composite systems. Moreover, the influence of the sulfide present in the sacrificial solution on the kinetics of the hydrogen evolution reaction on Pt particles or the reduction of holes in the valence band of sulfide can be excluded as well. This is because platinized sulfides, except for p-CdS, were more active than the composites in the same sacrificial solution (Table 2) and S^{2-} did not affect the photocatalytic activity of Pt-TiO_2 (Fig. S9, Supporting Information); note that these samples did not deactivate.

Scheme 1 shows that the transport of the electrons injected in TiO_2 to Pt centers (process V) is another parameter that influences the photocatalytic activity of the composite system. All studied composite materials share the use of TiO_2 P25 independent of the sulfide composition and preparation method. It is known that the mobility of conduction band electrons in TiO_2 is low due to the trapping/detrapping transport mechanism [49], which limits the performance of, for instance, TiO_2-based dye-sensitized solar cells [50]. The conclusion that the performance of the studied composites is limited by slow electron transport in TiO_2 may seem contradictory to the high activity of Pt-TiO_2 photocatalysts under UV irradiation (Fig. S9, Supporting Information). However, one should take into account that in these two instances conduction band electrons are generated in a different way. Excitation of Pt-TiO_2 with UV light ($\lambda < 400$ nm) leads to the formation of electron-hole pairs close to the surface of a particle where electrons can reach nearby Pt clusters and facilitate water reduction reaction and holes oxidize the sacrificial reagents. On the contrary, for composite photocatalysts (Scheme 1) visible light excitation ($\lambda > 420$ nm) generates charge carriers in sulfides particles and not in TiO_2. Then the holes oxidize sacrificial reagents and part of electrons facilitate reduction of water on the sulfide surface, while the rest is transferred to the conduction band of TiO_2 [19]. If the sulfide-oxide interface is far from the Pt centers, then the low mobility of electrons hampers their diffusion to hydrogen evolution centers and limits photocatalytic activity of the material.

The detrimental effect of the low electron mobility in TiO_2 was most evident for the h-$Cd_{0.5}Zn_{0.5}S$@Pt-TiO_2 due to the high photocatalytic activity of bare h-$Cd_{0.5}Zn_{0.5}S$ (Table 1). However, the deteriorating effect of Pt-TiO_2 on h-CdS or p-$Cd_{0.5}Zn_{0.5}S$ becomes apparent only when the activities of these platinized sulfides are taken into account (Table 2). p-CdS was the only sample, for which formation of the composite with Pt-TiO_2 had a positive effect. The intrinsic activity of this sulfide was the lowest (Table 2). Thus, the heterojunction with Pt-TiO_2 substantially improved charge separation and overall photocatalytic activity of the material in correspondence with literature [28,29]. Yet, we argue that this positive effect for this particular sample veils the limitations of the studied approach for the optimization of the activity of the transition sulfide-based composite photocatalyst in the water reduction reaction.

4. Conclusions

The visible-light driven photocatalytic reduction of water with composite materials consisting of transition metal sulfides and Pt-TiO_2 was investigated in detail. All composites with Pt-TiO_2 demonstrated similar activities despite the differences in their bandgaps, BET surface areas, transfer of conduction band electrons and intrinsic activities of sulfides. Moreover, in all cases, except for precipitated CdS, sulfide/Pt-TiO_2 composite photocatalysts were substantially less active than the corresponding standalone platinized sulfides. The systematic study revealed that efficiency of the composite materials was hampered by the low mobility of the conduction band electrons in TiO_2. In addition to this, we found that the mechanism of photocatalytic water reduction on CdS- and $Cd_{0.5}Zn_{0.5}S$-based materials was different. The CdS/Pt-TiO_2 system is sensitive to Pt poisoning, because the conduction band electrons in CdS have a low driving force toward water reduction and substantial part of hydrogen is produced on the Pt-TiO_2 component rather than on sulfide particles. Bare Cd-Zn sulfides have substantially higher photocatalytic activity toward the hydrogen evolution reaction. Therefore, in $Cd_{0.5}Zn_{0.5}S$-based composites sulfide particles compete with Pt-TiO_2 in water reduction making these photocatalysts less sensitive to the state of Pt.

Acknowledgements

The authors thank MSc. Bjorn Joos for the preliminary experiments for this study and Adelheid Elemans–Mehring for the ICP-OES analysis. This work is supported by NanoNextNL, a micro and nanotechnology consortium of the Government of The Netherlands and 130 partners: project NNNL.02B.08 CO2Fix-1.

Appendix A. Supplementary data

Supplementary data associated with this article can be found, in the online version, at http://dx.doi.org/10.1016/j.apcatb.2016.05.035.

References

[1] IEA, Solar Energy Perspectives, OECD Publishing, Paris, 2011.
[2] B.A. Pinaud, J.D. Benck, L.C. Seitz, A.J. Forman, Z. Chen, T.G. Deutsch, B.D. James, K.N. Baum, G.N. Baum, S. Ardo, H. Wang, E. Miller, T.F. Jaramillo, Energy Environ. Sci. 6 (2013) 1983–2002.
[3] J. Sabaté, S. Cervera-March, R. Simarro, J. Giménez, Chem. Eng. Sci. 45 (1990) 3089–3096.
[4] V.M. Daskalaki, M. Antoniadou, G. Li Puma, D.I. Kondarides, P. Lianos, Environ. Sci. Technol. 44 (2010) 7200–7205.
[5] J.A. Villoria, R.M. Navarro Yerga, S.M. Al-Zahrani, J.L.G. Fierro, Ind. Eng. Chem. Res. 49 (2010) 6854–6861.
[6] L. Huang, J. Yang, X. Wang, J. Han, H. Han, C. Li, Phys. Chem. Chem. Phys. 15 (2013) 553–560.
[7] A. Kudo, M. Sekizawa, Catal. Lett. 58 (1999) 241–243.
[8] X. Zhang, D. Jing, M. Liu, L. Guo, Catal. Commun. 9 (2008) 1720–1724.
[9] J. Zhang, S. Liu, J. Yu, M. Jaroniec, J. Mater. Chem. 21 (2011) 14655–14662.
[10] Y. Wang, Y. Wang, R. Xu, J. Phys. Chem. C 117 (2013) 783–790.
[11] J. Yang, H. Yan, X. Wang, F. Wen, Z. Wang, D. Fan, J. Shi, C. Li, J. Catal. 290 (2012) 151–157.
[12] J.C. Kim, J. Choi, Y.B. Lee, J.H. Hong, J.I. Lee, J.W. Yang, W.I. Lee, N.H. Hur, Chem. Commun. (Camb) (2006) 5024–5026.
[13] J.S. Jang, S.M. Ji, S.W. Bae, H.C. Son, J.S. Lee, J. Photochem. Photobiol. A Chem. 188 (2007) 112–119.
[14] H. Wang, L. Zhang, Z. Chen, J. Hu, S. Li, Z. Wang, J. Liu, X. Wang, Chem. Soc. Rev. 43 (2014) 5234–5244.
[15] R. Marschall, Adv. Funct. Mater. 24 (2014) 2421–2440.
[16] N. Serpone, E. Borgarello, M. Grätzel, J. Chem. Soc. Chem. Commun. (1984) 342–344.
[17] M. Qorbani, N. Naseri, O. Moradlou, R. Azimirad, A.Z. Moshfegh, Appl. Catal. B Environ. 162 (2015) 210–216.
[18] W. Dong, F. Pan, L. Xu, M. Zheng, C.H. Sow, K. Wu, G.Q. Xu, W. Chen, Appl. Surf. Sci. 349 (2015) 279–286.
[19] S.J.A. Moniz, S.A. Shevlin, D.J. Martin, Z.-X. Guo, J. Tang, Energy Environ. Sci. 8 (2015) 731–759.
[20] Y. Chen, L. Guo, J. Mater. Chem. 22 (2012) 7507–7514.
[21] J.S. Jang, H.G. Kim, U. a. Joshi, J.W. Jang, J.S. Lee, Int. J. Hydrogen Energy 33 (2008) 5975–5980.
[22] M. Antoniadou, V.M. Daskalaki, N. Balis, D.I. Kondarides, C. Kordulis, P. Lianos, Appl. Catal. B Environ. 107 (2011) 188–196.
[23] Q. Li, B. Guo, J. Yu, J. Ran, B. Zhang, H. Yan, J.R. Gong, J. Am. Chem. Soc. 133 (2011) 10878–10884.
[24] J. Zhang, J. Yu, M. Jaroniec, J.R. Gong, Nano Lett. 12 (2012) 4584–4589.
[25] Q. Li, H. Meng, P. Zhou, Y. Zheng, J. Wang, J. Yu, J. Gong, ACS Catal. 3 (2013) 882–889.
[26] C. Xing, Y. Zhang, W. Yan, L. Guo, Int. J. Hydrogen Energy 31 (2006) 2018–2024.
[27] L. Wang, W. Wang, M. Shang, W. Yin, S. Sun, L. Zhang, Int. J. Hydrogen Energy 35 (2010) 19–25.
[28] H. Park, W. Choi, M.R. Hoffmann, J. Mater. Chem. 18 (2008) 2379–2385.
[29] H. Park, Y.K. Kim, W. Choi, J. Phys. Chem. C 115 (2011) 6141–6148.
[30] A. Litke, J.P. Hofmann, T. Weber, E.J.M. Hensen, Inorg. Chem. 54 (2015) 9491–9498.
[31] L. Vegard, Zeitschrift Für Phys. 5 (1921) 17–26.

[32] M. Matsumura, S. Furukawa, Y. Saho, H. Tsubomura, J. Phys. Chem. 89 (1985) 1327–1329.
[33] N. Bao, L. Shen, T. Takata, K. Domen, A. Gupta, K. Yanagisawa, C. a. Grimes, J. Phys. Chem. C 111 (2007) 17527–17534.
[34] P. Scherrer, Nachr ges wiss goettingen, Math-Phys. Kl. (1918) 98–100.
[35] G.K. Williamson, W.H. Hall, Acta Metall. 1 (1953) 22–31.
[36] E. Estevez-Rams, A. Penton Madrigal, P. Scardi, M. Leoni, Zeitschrift Für Krist (Suppl. (1)) (2007) 99–104.
[37] H.M. Rietveld, J. Appl. Crystallogr. 2 (1969) 65–71.
[38] S. Trasatti, J. Electroanal. Chem. Interfacial Electrochem. 39 (1972) 163–184.
[39] Y. Xu, M.A.A. Schoonen, Am. Mineralogist 85 (2000) 543–556.
[40] W. Bremser, New Methods Chem, Springer-Verlag, Berlin/Heidelberg, 1973, pp. 1–37.
[41] B.C. Beard, P.N. Ross, J. Phys. Chem. 90 (1986) 6811–6817.
[42] J.C. Colmenares, A. Magdziarz, M. a. Aramendia, A. Marinas, J.M. Marinas, F.J. Urbano, J. a. Navio, Catal. Commun. 16 (2011) 1–6.
[43] Y. Zhou, C.L. Menéndez, M.J.-F. Guinel, E.C. Needels, I. González-González, D.L. Jackson, N.J. Lawrence, C.R. Cabrera, C.L. Cheung, RSC Adv. 4 (2014) 1270–1275.
[44] H. Gao, W. Xu, H. He, X. Shi, X. Zhang, K. Tanaka, Spectrochim. Acta Part A Mol. Biomol. Spectrosc. 71 (2008) 1193–1198.
[45] E.V. Benvenutti, L. Franken, C.C. Moro, C.U. Davanzo, Langmuir 15 (1999) 8140–8146.
[46] C. Deiana, E. Fois, S. Coluccia, G. Martra, J. Phys. Chem. C 114 (2010) 21531–21538.
[47] K. Ding, A. Gulec, A.M. Johnson, N.M. Schweitzer, G.D. Stucky, L.D. Marks, P.C. Stair, Science 350 (2015) 189–192.
[48] J.K. Dunleavy, Platin. Met. Rev. 50 (2006), 110–110.
[49] X. Wang, G. Liu, Z.-G. Chen, F. Li, L. Wang, G.Q. Lu, H.-M. Cheng, Chem. Commun. (Camb). (2009) 3452–3454.
[50] A.K. Chandiran, M. Abdi-Jalebi, M.K. Nazeeruddin, M. Grätzel, ACS Nano 8 (2014) 2261–2268.